Dynamical Tides in Eccentric, Massive Stellar Binaries

The Authors

Accepted XXX. Received YYY; in original form ZZZ

ABSTRACT

The long-term orbital evolution of binaries in which at least one component is a massive, main-sequence star is predominantly due to dynamical tides. However, most understanding of dynamical tides is only applicable when the binary is nearly circular. In this work, we study the effect of dynamical tides in massive stellar binaries with large eccentricities and derive analytical expressions for the orbital decay, circularization, and spin synchronization rates. We apply our results to the radio pulsar J0045-7319, which has a massive B star companion and a rapidly decreasing orbital period. In order to reproduce the measured orbital decay via dynamical tides, we find that the core is likely rotating significantly faster than the measured surface rotation rate. This tentatively suggests a long core-envelope coupling timescale in the B star in J0045-7319. Our analytical approach can also be applied to other scenarios of tidal dissipation in eccentric binaries.

Key words: keywords

1 INTRODUCTION

The physics of tidal dissipation in massive, main-sequence (MS) stars (i.e. having a convective core and radiative envelope) under the gravitational influence of a companion was first studied by Zahn (1975) (see also Savonije & Papaloizou 1983; Goldreich & Nicholson 1989). The dominant dissipation mechanism is through the *dynamical tide*, in which the time-dependent tidal potential of the companion excites internal gravity waves at the radiative-convective boundary (RCB). As the wave propagates towards the surface, its amplitude grows, and the wave dissipates efficiently (Zahn 1975; Goldreich & Nicholson 1989; Su et al. 2020). The contribution due to the *equilibrium tide*, in which the tidal potential induces a static deformation of the star that undergoes viscous dissipation (see e.g. Alexander 1973; Hut 1981), is expected to be subdominant to the dynamical tide in stars with radiative envelopes (Zahn 1977; Goldreich & Nicholson 1989). (NB for Dong: Vigna-Gómez et al. (2020) say that the dynamical tide is less efficient in virtually all binaries, are there any recent references for the strength of the dynamical tide in stars with radiative envelopes?)

The original expression describing the torque due to dynamical tides by Zahn (1975) is very sensitive to the global properties of the star. Kushnir et al. (2017) present an updated derivation of the tidal torque dependent only on the local stellar properties near the RCB, eliminating many uncertainties from the Zahn's original expression. In Zaldarriaga et al. (2018), the authors use the new expression to study tidal synchronization in binaries consisting of a Wolf-Rayet star and a black hole, progenitors to black hole binaries that may be observed by LIGO/VIRGO.

These previous works all apply to circular binaries. However, massive stars can be found in high-eccentricity (high-e) systems, such as binaries consisting of one MS star and one neutron star (NS). The NS is formed with a large kick, giving rise to a high-e binary. Several such high-e systems have been discovered (e.g. Johnston et al. 1994; Bell et al. 1995; Champion et al. 2008). An important issue is to understand whether such high-e systems can circularize prior to mass transfer or a common envelope phase (Vigna-Gómez et al. 2020).

The purpose of this paper is to derive an analytical expression for the effect of dynamical tides for high-e binaries with a massive MS star. In Section 2, we review the effect of dynamical tides in circular binaries and existing techniques for studying high-e systems. In Section 3, we evaluate the effect of dynamical tides in high-e systems containing a massive MS star, including the torque and orbital decay rate. In Section 4, we apply our results to the pulsar-MS binary J0045-7319, for which a non-zero orbital decay rate has been measured. Finally, we summarize and discuss in Section 5.

2 DYNAMICAL TIDES IN MASSIVE STARS

2.1 Circular Orbit

We first review the case where the binary is circular. Let M be the mass of the MS star, M_2 the mass of the companion, a the semimajor axis of the binary, and Ω the mean motion of the binary. The tidal torque exerted on the star by the companion is (Kushnir et al. 2017):

$$T_{\rm circ}(\omega) = T_0 \,\mathrm{sgn}\,(\omega) \left|\frac{\omega}{\Omega}\right|^{8/3}, \tag{1}$$

$$T_0 \equiv \beta_2 \frac{G M_2^2 r_{\rm c}^5}{a^6} \left(\frac{\Omega}{\sqrt{G M_{\rm c}/r_{\rm c}^3}}\right)^{8/3} \frac{\rho_{\rm c}}{\bar{\rho}_{\rm c}} \left(1 - \frac{\rho_{\rm c}}{\bar{\rho}_{\rm c}}\right)^2, \tag{2}$$

$$\beta_2 \equiv \left[\frac{r_{\rm c}}{g_{\rm c}} \left(\frac{{\rm d}N^2}{{\rm d}\ln r}\right)_{r=r_{\rm c}}\right]^{-1/3} \left[\frac{3}{2} \frac{3^{2/3}\Gamma^2(1/3)}{5 \cdot 6^{4/3}} \frac{3}{4\pi} \alpha^2\right]. \tag{3}$$

Here, $\omega \equiv 2\Omega - 2\Omega_{\rm s}$ is the tidal forcing frequency, $\Omega_{\rm s}$ is the spin of the MS star, N is the Brünt-Vaisala frequency, r is the radial coordinate within the star, and $r_{\rm c}$, $M_{\rm c}$, $g_{\rm c}$, $\rho_{\rm c}$, and $\bar{\rho}_{\rm c}$ are the radius of the RCB, the mass contained within the convective core, the gravitational acceleration at the RCB, the stellar density at the RCB, and the average density of the convective core respectively. α is a numerical

constant of order unity given by Eq. (A32) of Kushnir et al. (2017), and $\beta_2 \approx 1$ for a large range of stellar models (Fig. 2 of Kushnir et al. 2017). In Eq. (1), we have written the terms such that T_0 contains all the spin-independent terms.

Note that we use Eq. (1) from Kushnir et al. (2017) instead of the classic expression from Zahn (1975), which is given by:

$$T_{\rm circ}^{\rm (Zahn)}(\omega) = \frac{3}{2}\frac{GM^2R^5}{a^6}E_2\omega^{8/3}, \tag{4}$$

where M and R are the mass and radius of the MS star and E_2 is a numerical parameter obtained by integrating over the entire star. The fitting formula $E_2 = 1.592\times10^{-9}\,(M/M_\odot)^{2.84}$ as given by Hurley et al. (2002) is commonly used, which varies by many orders of magnitude for different stars. Moreover, $T_{\rm circ}^{\rm (Zahn)}$ depends on M and R, properties of the entire star, when the tidal torque is entirely generated at the RCB. For these reasons, the expression by Kushnir et al. (2017) is preferred.

2.2 Eccentric Binaries

The gravitational potential of an eccentric companion at the quadrupole order can be decomposed as a sum over circular orbits (e.g. Storch & Lai 2013; Vick et al. 2017):

$$U = \sum_{m=-2}^{2} U_{2m}(\vec{r},t), \tag{5}$$

$$\begin{aligned} U_{2m}(\vec{r},t) &= -\frac{GM_2W_{2m}r^2}{D(t)^3}Y_{2m}(\theta,\phi)e^{-imf(t)}, \\ &= -\frac{GM_2W_{2m}r^2}{a^3}Y_{2m}(\theta,\phi)\sum_{N=-\infty}^{\infty}F_{Nm}e^{-iN\Omega t}. \end{aligned} \tag{6}$$

Here, the coordinate system is centered on the MS star, (r,θ,ϕ) are the radial, polar, and azimuthal coordinates of $\vec{r}$ respectively, $W_{2\pm2} = \sqrt{3\pi/10}, W_{2\pm1} = 0, W_{20} = -\sqrt{\pi/5}$, $D(t)$ is the instantaneous distance to the companion, f is the true anomaly, and Y_{lm} denote the spherical harmonics. F_{Nm} denote the *Hansen coefficients* for $l = 2$ (also denoted X_{2m}^n in Murray & Dermott 1999), which are the Fourier coefficients of the perturbing function, i.e.

$$\frac{a^3}{D(t)^3}e^{-imf(t)} = \sum_{N=-\infty}^{\infty}F_{Nm}e^{-iN\Omega t}. \tag{7}$$

The F_{Nm} can be written explicitly as an integral over the eccentric anomaly (Murray & Dermott 1999; Storch & Lai 2013):

$$F_{Nm} = \frac{1}{\pi}\int_0^\pi \frac{\cos\left[N(E-e\sin E)-mf(E)\right]}{(1-e\cos E)^2}\,{\rm d}E. \tag{8}$$

By considering the effect of each summand in Eq. (5), the total torque on the star, energy transfer in the inertial frame, and heating in the star's corotating frame can be obtained (Storch & Lai 2013; Vick et al. 2017):

$$T = \sum_{N=-\infty}^{\infty}F_{N2}^2T_{\rm circ}(N\Omega-2\Omega_{\rm s}), \tag{9}$$

$$\begin{aligned} \dot{E}_{\rm in} = \frac{1}{2}\sum_{N=-\infty}^{\infty}\Bigg\{&\left(\frac{W_{20}}{W_{22}}\right)^2 N\Omega F_{N0}^2T_{\rm circ}(N\Omega) \\ &+ N\Omega F_{N2}^2T_{\rm circ}(N\Omega-2\Omega_{\rm s})\Bigg\}, \end{aligned} \tag{10}$$

$$\dot{E}_{\rm rot} = \dot{E}_{\rm in} - \Omega_{\rm s}T. \tag{11}$$

Here, dots indicate time derivatives.

These can be used to express the binary orbital decay and circularization times using:

$$\frac{\dot{a}}{a} = -\frac{2a\dot{E}_{\rm in}}{GMM_2}, \tag{12}$$

$$\frac{\dot{e}e}{1-e^2} = -\frac{a\dot{E}_{\rm in}}{GMM_2} + \frac{T}{L_{\rm orb}}, \tag{13}$$

where $L_{\rm orb} = MM_2\left[Ga(1-e^2)/(M+M_2)\right]^{1/2}$ is the orbital angular momentum. The stellar synchronization time can also be computed assuming that the star rotates rigidly:

$$\dot{\Omega}_{\rm s} = \frac{T}{kMR^2}, \tag{14}$$

where kMR^2 is the moment of inertia of the MS star.

3 ANALYTIC EVALUATION OF TIDAL TORQUE AND ENERGY TRANSFER

We can combine the results given in Sections 2.1 and 2.2 to compute the torque and energy transfer rate due to dynamical tides in an eccentric binary. The tidal torque is obtained by evaluating Eq. (9) with the circular torque set to Eq. (1), giving:

$$T = \sum_{N=-\infty}^{N=\infty}F_{N2}^2T_0\,{\rm sgn}\left(N-\frac{2\Omega_{\rm s}}{\Omega}\right)\left|N-\frac{2\Omega_{\rm s}}{\Omega}\right|^{8/3}. \tag{15}$$

The energy transfer rate in the inertial frame is obtained by evaluating Eq. (10) in the same way, giving:

$$\begin{aligned} \dot{E}_{\rm in} = \frac{T_0}{2}\sum_{N=-\infty}^{\infty}\Bigg[&N\Omega F_{N2}^2{\rm sgn}\left(N-2\Omega_{\rm s}/\Omega\right)|N-2\Omega_{\rm s}/\Omega|^{8/3} \\ &+\left(\frac{W_{20}}{W_{22}}\right)^2\Omega F_{N0}^2|N|^{11/3}\Bigg]. \end{aligned} \tag{16}$$

These two expressions can be used to obtain the orbital decay, circularization, and spin synchronization timescales using Eqs. (12–14).

While exact, these two sums are difficult to evaluate for larger eccentricities, where one often must sum hundreds or thousands of terms, each of which has a different F_{Nm}. In the following sections, our objective is to obtain closed-form approximations to Eqs. (15–16) when the eccentricity is sufficiently large that the sums cannot be approximated by just one or two terms.

3.1 Approximating Hansen Coefficients

Towards simplifying Eqs. (15–16), we seek tractable approximations for both F_{N2} and F_{N0}. Note that while the Hansen coefficients can be evaluated using the integral expression Eq. (8), this requires calculating a separate integral for each N. Instead, it is more convenient to use the discrete Fourier Transform of the left hand side of Eq. (7) to calculate arbitrarily many N at once (as pointed out by Correia et al. 2014). Since $F_{(-N)m} = F_{N(-m)}$, we will only study the Hansen coefficient behavior for $m \geq 0$.

3.1.1 $m = 2$ *Hansen Coefficients*

Figure 1 shows the F_{N2} when $e = 0.9$. First, we note that F_{N2} is much larger when $N \geq 0$ than for $N < 0$, so we focus on the behavior for $N \geq 0$. Here, F_{N2} has only one substantial peak. There

are only two characteristic frequency scales: Ω and Ω_p the pericenter frequency, defined by

$$\Omega_p \equiv \Omega \frac{\sqrt{1+e}}{(1-e)^{3/2}}. \tag{17}$$

For convenience, we also define N_p as the floor of Ω_p/Ω, i.e.

$$N_p \equiv \lfloor \Omega_p/\Omega \rfloor, \tag{18}$$

We find that the peak of the F_{N2} occurs at $\sim N_p$, the only characteristic scale in N over which F_{N2} can vary. When $N \gg N_p$, the Fourier coefficients must fall off exponentially by the Paley-Wiener theorem, as the left hand side of Eq. (7) is smooth (e.g. Stein & Shakarchi 2009). When instead $N \ll N_p$, there are no characteristic frequencies between Ω and Ω_p, so we expect the Hansen coefficients to be free between $N = 1$ and N_p, i.e. a power law in N. The expected behaviors in both of these regimes are in agreement with Fig. 1.

Motivated by these considerations, we assume the Hansen coefficients can be approximated by a function of form:

$$F_{N2} \approx \begin{cases} C_2 N^p e^{-N/\eta_2} & N \geq 0, \\ 0 & N < 0, \end{cases} \tag{19}$$

for some fitting coefficients C_2, p, and η_2. By performing fits to F_{N2}, we found that $p \approx 2$ for substantial eccentricities, and we take $p = 2$ to be fixed for the remainder of this work[1].

To constrain the remaining two free parameters η_2 and C_2 the normalization, we use the well known Hansen coefficient moments (Hut 1981)

$$\sum_{N=-\infty}^{\infty} F_{N2}^2 = \frac{f_5}{(1-e^2)^{9/2}}, \tag{20}$$

$$f_5 \equiv 1 + 3e^2 + \frac{3e^4}{8}, \tag{21}$$

$$\sum_{N=-\infty}^{\infty} F_{N2}^2 N = \frac{2 f_2}{(1-e^2)^6}, \tag{22}$$

$$f_2 \equiv 1 + \frac{15e^2}{2} + \frac{45e^4}{8} + \frac{5e^6}{16}. \tag{23}$$

We have defined the common functions f_2 and f_5. This fixes

$$\eta_2 = \frac{4 f_2}{5 f_5 (1-e^2)^{3/2}}, \tag{24}$$

$$C_2 = \left[\frac{4 f_5}{3 (1-e^2)^{9/2} \eta_2^5} \right]^{1/2}. \tag{25}$$

Figure 1 illustrates the aggrement of Eq. (19) using these two values

[1] There is good reason to expect that $p = 2$ for $N \ll N_p$ as long as the eccentricity is sufficiently large, as then the left hand side of Eq. (7) resembles the second derivative of a Dirac delta function within each orbital period: It is both sharply peaked about $t = 0$ and has zero derivative three times every period (at $t = \epsilon$, $t = P/2$, and $t = P - \epsilon$ for some small $\epsilon \sim \Omega_p^{-1}$). These two characteristics describe the second derivative of a Gaussian with width $\sim \Omega_p^{-1}$. Then, for timescales longer than its width, a Gaussian resembles a Dirac delta function, which has a flat Fourier spectrum ($\propto N^0$). Finally, since time differentiation multiplies by N in frequency space, the second derivative of a Gaussian has a Fourier spectrum $\propto N^2$ for sufficiently small $N \lesssim N_p$. As F_{N2} is the Nth Fourier coefficient for a function resembling the second derivative of a Dirac delta function for $N \lesssim N_p$, we do indeed expect $F_{N2} \propto N^2$ in this regime.

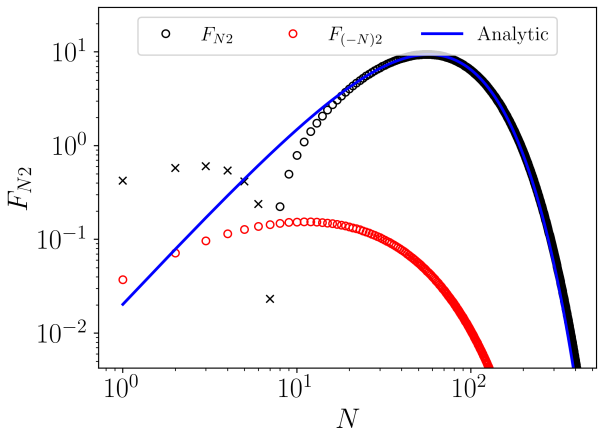

Figure 1. Plot of Hansen coefficients F_{N2} for $e = 0.9$. The red circles denote negative N, while the black circles and crosses denote positive and negative F_{N2}. The blue line is the formula given by Eq. (19) with η_2 and C_2 given by Eqs. (24–25).

of η_2 and C_2 with the numerical F_{N2}. The good agreement is especially impressive as there are no fitting parameters in Eq. (19), as C_2, η_2, and p are all analytically constrained. Finally, note that the maximum of the F_{N2} occurs at $N = \lfloor 2\eta_2 \rfloor$, and $2\eta_2 \propto (1-e)^{3/2} \Omega_p$, so the maximum occurs at $N \sim N_p$ as argued above.

3.1.2 $m = 0$ *Hansen Coefficients*

We now turn to the $m = 0$ Hansen coefficients, F_{N0}, which are shown in Fig. 2. We know that $F_{N0} = F_{(-N)0}$, so we consider only $N \geq 0$. From the figure, we see that the F_{N0} decay exponentially. There is only one characteristic scale available for this decay, namely N_p. Therefore, we naturally assume the F_{N0} coefficients can be approximated by a function of form:

$$F_{N0} = C_0 e^{-|N|/\eta_0}. \tag{26}$$

The two free parameters C_0 and η_0 are constrained by the well known moments (Hut 1981)

$$\sum_{N=-\infty}^{\infty} F_{N0}^2 = \frac{f_5}{(1-e^2)^{9/2}}, \tag{27}$$

$$\sum_{N=-\infty}^{\infty} F_{N0}^2 N^2 = \frac{9e^2}{2(1-e^2)^{15/2}} f_3, \tag{28}$$

$$f_3 = \frac{1}{2} + \frac{15e^2}{8} + \frac{15e^4}{16} + \frac{5e^6}{128}. \tag{29}$$

We have defined the common function f_3. This then requires

$$\eta_0 = \left[\frac{9e^2 f_3}{(1-e^2)^3 f_5} \right]^{1/2}, \tag{30}$$

$$C_0 = \left[\frac{f_5}{(1-e^2)^{9/2} \eta_0} \right]^{1/2}. \tag{31}$$

Figure 2 illustrates the agreement of Eq. (26) using these two values of η_0 and C_0, where again good agreement is observed.

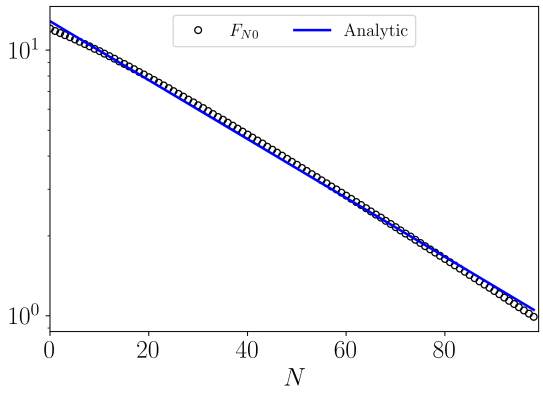

Figure 2. Plot of F_{N0} (black circles) for $e = 0.9$. Since $F_{N0} = F_{(-N)0}$, we only show positive N. The blue line is given by Eq. (26) with η_0 and C_0 given by Eqs. (30–31).

3.2 Approximate Expressions for Torque and Energy Transfer

Having found good approximations for the Hansen coefficients, we now apply them to simplify the formulas for the torque and the energy transfer rate in Eqs. (15–16).

3.2.1 Tidal Torque

To simplify the torque, given by Eq. (15), we replace F_{N2} with Eq. (19) and the sum with an integral, obtaining

$$T \approx T_0 \int_0^\infty C_2^2 N^4 e^{-2N/\eta_2} \operatorname{sgn}(N - 2\Omega_s/\Omega) \, |N - 2\Omega_s/\Omega|^{8/3} \, \mathrm{d}N. \tag{32}$$

This expression is already easier to evaluate than Eq. (15), but we can use further approximations to obtain a closed form. We first analyze Eq. (32) in the zero spin limit, where it can be integrated analytically[2], giving

$$\lim_{\Omega_s \to 0} T = T_0 \frac{f_5 (\eta_2/2)^{8/3}}{(1-e^2)^{9/2}} \frac{\Gamma(23/3)}{4!}. \tag{33}$$

Note that this has the expected scaling $T \sim T_p \Omega/\Omega_p$, where T_p is the torque exerted by a circular orbit with separation equal to the pericenter separation $a_p \equiv a(1-e)$, i.e.

$$T_p = \beta_2 \frac{G M_2^2 r_c^5}{a_p^6} \left(\frac{\Omega_p}{\sqrt{G M_c / r_c^3}} \right)^{8/3} \frac{\rho_c}{\bar{\rho}_c} \left(1 - \frac{\rho_c}{\bar{\rho}_c}\right)^2. \tag{34}$$

The top panel of Fig. 3 compares this formula to the integral of Eq. (32) and to the direct sum of Eq. (15) as a function of the eccentricity. It can be see that both the integral and the analytic closed form perform well for moderate-to-large eccentricities, but both overpredict the torque at small $e \lesssim 0.3$. This discrepancy is expected: there are only a few nonnegligible summands in Eq. (15) when e is small, so replacing the sum over N with an integral is expected to introduce significant inaccuracy that appears in both the integral and closed form expression.

Eq. (33) is valid so long as $|\Omega_s/\Omega| \ll N_{\max}$, where $N_{\max} = 10\eta_2/3$ is where the integrand is maximized. If instead $|\Omega_s/\Omega| \gg N_{\max}$, the torque can be evaluated directly using Eq. (15) and the known Hansen coefficient moments, giving:

$$\lim_{\Omega_s \to \infty} T = -T_0 \operatorname{sgn}(\Omega_s) \; |2\Omega_s/\Omega|^{8/3} \frac{f_5}{(1-e^2)^{9/2}}. \tag{35}$$

The bottom panel of Fig. 3 compares this formula to the integral of Eq. (32) and to the direct sum of Eq. (15) as a function of the eccentricity, where $\Omega_s/\Omega = 400$. Here, $400 \gg N_{\max}$ for all eccentricities shown. We see that direct summation, the integral expression, and Eq. (35) all agree very well for all eccentricities.

We now have obtained the asymptotic forms of Eq. (32) for small and large spins, but we can further derive a single expression joining these two limits. To do this, we first assume that the spin is small but non-negligible. In this regime, we make the approximation

$$N - 2\Omega_s/\Omega \simeq \frac{N}{N_{\max}} \left(N_{\max} - \frac{2\gamma_T \Omega_s}{\Omega} \right), \tag{36}$$

for some free parameter γ_T, after which we can integrate Eq. (32) in closed form. γ_T is fixed by requiring our expression reproduce the large spin limit (Eq. 35) when taking $|\Omega_s| \to \infty$. This procedure gives an expression for the torque that agrees with both asymptotic forms (Eq. 35–33) and is given by:

$$T = T_0 \frac{f_5 (\eta_2/2)^{8/3}}{(1-e^2)^{9/2}} \operatorname{sgn}\left(1 - \gamma_T \frac{\Omega_s}{\eta_2 \Omega}\right) \left| \frac{4}{\gamma_T} \left(1 - \gamma_T \frac{\Omega_s}{\eta_2 \Omega}\right) \right|^{8/3}, \tag{37}$$

$$\gamma_T = 4 \left(\frac{4!}{\Gamma(23/3)} \right)^{3/8} \approx 0.691. \tag{38}$$

Figure 4 compares this expression to the integral of Eq. (32) and to the direct sum of Eq. (15) at fixed $e = 0.9$ and varying Ω_s. Eq. (37) agrees well with both the integral and sum for large and small spins, as is expected from how it is constructed, and is also somewhat accurate for intermediate spins. However, Eq. (32) is more accurate than Eq. (37) when T changes signs and $|T|$ is small. This is also expected: T changes signs when the spin approaches *pseudosynchronization* (Section 3.2.2) because large contributions to the sum in Eq. (15) have opposite signs and mostly cancel out. Thus, small inaaccuracies in the summand result in significant discrepancies in the total torque. The integral approximation, Eq. (32), is expected to be in good agreement with the direct sum, Eq. (15), as the accuracy of the Hansen coefficient approximation in Section 3.1 is good for large eccentricities, thus guaranteeing term-by-term accuracy. On the other hand, the closed form expression, Eq. (37), is a crude extrapolation where $|\Omega_s/\Omega| \simeq N_{\max}$ and is not expected to be accurate in this regime. In fact, Eq. (37) predicts that $\mathrm{d}T/\mathrm{d}\Omega_s \approx 0$ near pseudosynchronization. This is not accurate and is an artifact of our factorization ansatz in Eq. (42).

In summary, the tidal torque must be evaluated with explicit summation (Eq. 15) when $e \lesssim 0.3$ (see discussion after Eq. 33), can be approximated by the integral expression (Eq. 32) when e is large even when $\Omega_s \simeq \Omega_p$, and otherwise can be approximated by the closed-form expression given by Eq. (37). Recall that when e is small, explicit summation of Eq. (15) is quite simple, as good accuracy can be obtained with just the first few terms in the summation.

[2] The key to the success of our approach is that sums of form $\sum_{n=-\infty}^{\infty} F_{N2}^2 N^p$ can be approximated for non-integer p in terms of Γ, since $\int_0^\infty x^p e^{-x} \, \mathrm{d}x = \Gamma(p-1)$. This is not possible with existing analytical techniques.

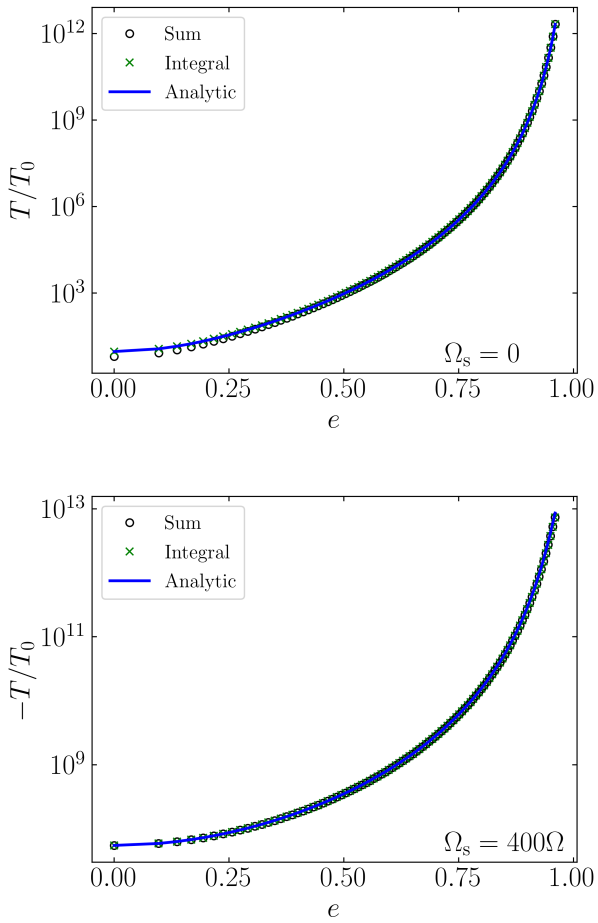

Figure 3. Tidal torque on a non-rotating (top) and rapidly rotating (bottom) star due to a companion with orbital eccentricity e. Black circles represent direct summation of Eq. (15), green crosses are evaluated using the integral approximation Eq. (32), and the blue line is Eq. (37). In the small and large spin limits, Eq. (37) reduces to Eq. (33) and Eq. (35) respectively.

3.2.2 *Pseudosynchronization*

In general, the exact torque as given by Eq. (15) vanishes for a single Ω_s, which we call the *pseudosynchronized* spin frequency. An approximation for the pseudosynchronized spin can be directly read off of Eq. (37):

$$\frac{\Omega_{ps}}{\Omega} = \frac{\eta_2}{\gamma_T} = \frac{4 f_2}{5\gamma_T f_5 \left(1-e^2\right)^{3/2}}. \tag{39}$$

This has the expected scaling $\Omega_{ps} \simeq \Omega_p$. Figure 5 compares these two predictions for the pseudosynchronized spin to the exact one obtained by applying a root finding algorithm to Eq. (15). We see that Ω_{ps} is a good approximation for the pseudosynchronized spin frequency when $e \lesssim 0.1$.

In passing, we note that, in the standard weak friction theory of equilibrium tides, the pseudosynchronized spin is given by (Alexander 1973; Hut 1981)

$$\frac{\Omega_{ps}^{(Eq)}}{\Omega} = \frac{f_2}{f_5 \left(1-e^2\right)^{3/2}}. \tag{40}$$

Though describing a different tidal phenomenon, this only differs from Eq. (39) by a factor of $4/(5\gamma_T) \approx 1.15$. We show it for comparison as the red dotted line in Fig. 5.

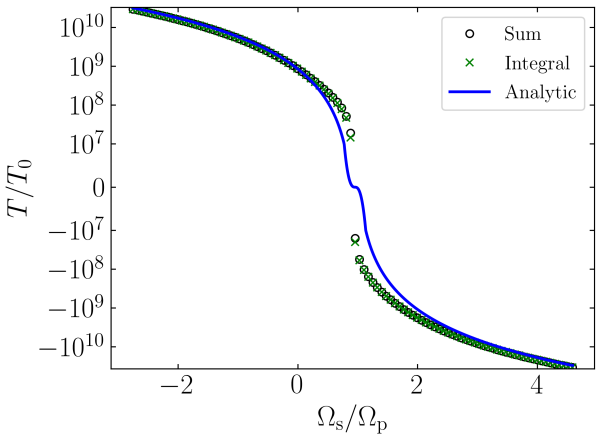

Figure 4. Tidal torque as a function of spin for a highly eccentric $e = 0.9$ companion. Black circles represent direct summation of Hansen coefficients (Eq. 15), green crosses the integral approximation (Eq. 32), and solid lines represent the analytic closed form (Eq. 37). The spin is normalized by $\Omega_p \approx 43\Omega$ (Eq. 17).

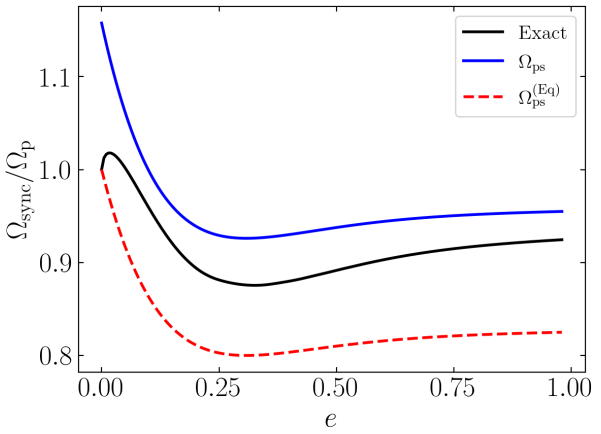

Figure 5. Calculations of the pseudosynchronization spin frequencies Ω_{sync} normalized by the pericenter frequency Ω_p (Eq. 17) as a function of eccentricity. The blue line is given by Eq. (39). The black line shows the exact solution, obtained using finding a root finding algorithm to solve for the zero of Eq. (9). The red dashed line shows the pseudosynchronization spin frequency predicted by the weak friction theory of equilibrium tides (Eq. 40).

3.2.3 Energy Transfer

We now turn our attention to Eq. (10) and replace F_{N2} and F_{N0} with their respective approximations (Eqs. 19 and 26) to obtain

$$\dot{E}_{\rm in} = \frac{T_0\Omega}{2}\int_0^\infty \left[C_2^2 N^5 e^{-2N/\eta_2}\,{\rm sgn}\left(N-2\Omega_{\rm s}/\Omega\right)\left|N-2\Omega_{\rm s}/\Omega\right|^{8/3} + 2\left(\frac{W_{20}}{W_{22}}\right)^2 C_0^2 e^{-2N/\eta_0} N^{11/3}\right] {\rm d}N. \tag{41}$$

We evaluate the $m = 2$ and $m = 0$ contributions to this expression separately.

We first examine the $m = 2$ contribution using the same procedure that was used in Section 3.2.1 for the torque. If the spin is moderate, i.e. $|\Omega_{\rm s}/\Omega| \lesssim N_{\rm max}$ where now $N_{\rm max} = 23\eta_2/6$, we make the approximation

$$N - 2\Omega_{\rm s}/\Omega \simeq \frac{N}{N_{\rm max}}\left(N_{\rm max} - \frac{2\gamma_E\Omega_{\rm s}}{\Omega}\right), \tag{42}$$

where γ_E is a free parameter. This lets us integrate the $m = 2$ component of Eq. (41) analytically. We constrain γ_E by requiring agreement with the large-spin limit, where $|\Omega_{\rm s}/\Omega| \gg N_{\rm max}$ and we obtain

$$\lim_{\Omega_{\rm s}\to\infty} \dot{E}_{\rm in}^{(m=2)} = -\frac{T_0\Omega}{2}\,{\rm sgn}(\Omega_{\rm s})|2\Omega_{\rm s}/\Omega|^{8/3}\frac{2f_2}{(1-e^2)^6}. \tag{43}$$

This fixes γ_E and we obtain the complete $m = 2$ contribution:

$$\dot{E}_{\rm in}^{(m=2)} = \frac{T_0\Omega f_5(\eta_2/2)^{11/3}}{2(1-e^2)^{9/2}} \times {\rm sgn}\left(1-\gamma_E\frac{\Omega_{\rm s}}{\eta_2\Omega}\right)\left|\frac{4}{\gamma_E}\left(1-\gamma_E\frac{\Omega_{\rm s}}{\eta_2\Omega}\right)\right|^{8/3}, \tag{44}$$

$$\gamma_E = 4\left(\frac{5!}{\Gamma(26/3)}\right)^{3/8} \approx 0.5886. \tag{45}$$

Note that, when $\Omega_{\rm s} \approx 0$, Eq. (44) gives the expected scaling of $\dot{E}_{\rm in}^{(m=2)} \sim T_{\rm p}\Omega$ where $T_{\rm p}$ is the torque exerted by a circular companion at the pericenter separation, given by Eq. (34).

The $m = 0$ contribution to Eq. (41) can be straightforwardly integrated using the parameterization Eq. (26). The sum of the two contributions then gives the total energy transfer rate:

$$\dot{E}_{\rm in} = \frac{T_0\Omega}{2}\left[\frac{f_5(\eta_2/2)^{11/3}}{(1-e^2)^{9/2}} \times {\rm sgn}\left(1-\gamma_E\frac{\Omega_{\rm s}}{\eta_2\Omega}\right)\left|\frac{4}{\gamma_E}\left(1-\gamma_E\frac{\Omega_{\rm s}}{\eta_2\Omega}\right)\right|^{8/3} + \frac{f_5\Gamma(14/3)}{(1-e^2)^{10}}\left(\frac{3}{2}\right)^{8/3}\left(\frac{e^2 f_3}{f_5}\right)^{11/6}\right]. \tag{46}$$

The two panels of Fig. 6 compare this expression with the integral form Eq. (41) and the direct sum Eq. (16) for small and large spins as a function of e. Again, when the spin and eccentricity are both negligible, both the integral and closed form expressions overpredict the energy dissipation rate. Figure 7 compares these three expressions as a function of spin when $e = 0.9$. The performance of the Eq. (46) degrades when the system is near pseudosynchronization, i.e. $\Omega_{\rm s} \simeq \Omega_{\rm p}$, but generally captures the correct scaling, while Eq. (41) is accurate for all spins. As was the case with the tidal torque, we see that evaluation of the energy transfer rate when $e \lesssim 0.3$ requires direct summation (Eq. 16), evaluation when e is substantial but the spin is near pseudosynchronization can be performed using the integral approximation (Eq. 41), and otherwise evaluation can be performed using the closed-form expression (Eq. 46).

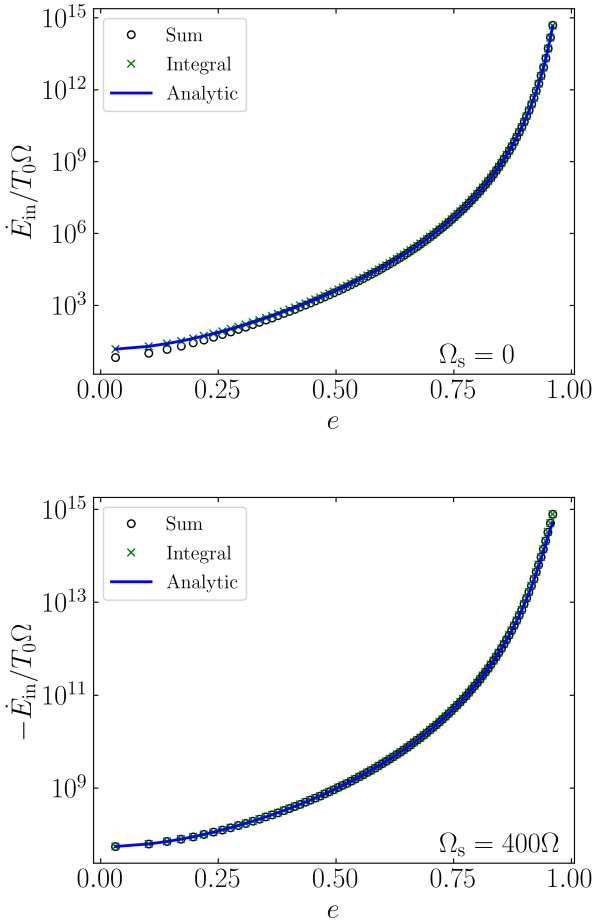

Figure 6. Plot of $\dot{E}_{\rm in}$ for a non-rotating (top) and a rapidly rotating (bottom) star. Black circles represent direct summation of the Hansen coefficients as in Eq. (16), green crosses the integral form Eq. (41), and the blue line the closed form Eq. (46).

4 EXAMPLE SYSTEM: PSR J0045+7319

As an example of our calculations above, we consider the pulsar-MS binary PSR J0045-7319 (Bell et al. 1995) and attempt to explain its orbital decay via dissipation due to dynamical tides. Previous attempts to do so used Zahn's parameterized theory of dynamical tides and thus are more susceptible to inaccuracies (e.g. Lai 1996; Kumar & Quataert 1998). The binary was initially reported to have pulsar mass $M_2 = 1.4M_\odot$, mass ratio $q = 6.3$, $e = 0.808$, orbital period $P = 51.17$ days, and exhibit orbital decay at the rate $\dot{P} = -3.03\times10^{-7}$ (Kaspi et al. 1996). From these, a MS mass of $M = 8.8M_\odot$ and an orbital separation of $a = 126R_\odot$ can be inferred. Furthermore, the measured luminosity $L = 1.2\times10^4 L_\odot$ and surface temperature $T_{\rm surf} = (24000\pm1000)$ K of the MS star its radius to be

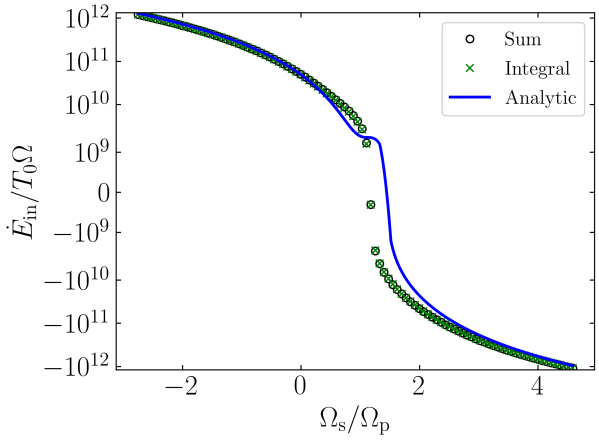

Figure 7. $\dot{E}_{\rm in}$ as a function of spin [normalized by $\Omega_{\rm p}$; Eq. (17)] for a highly eccentric $e = 0.9$ companion. Black circles represent direct summation of Hansen coefficients, green crosses the integral approximation, and the blue line the analytic closed form.

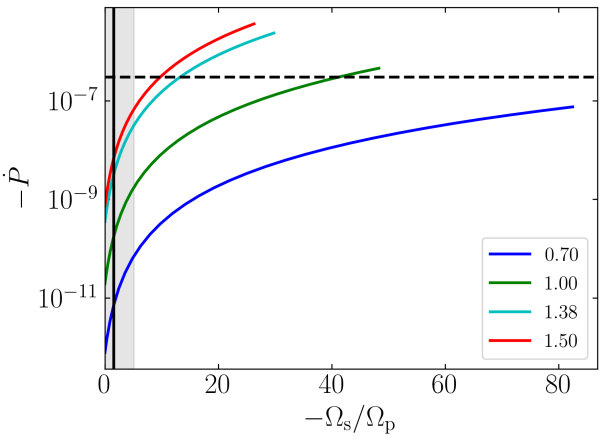

Figure 8. $\dot{P}$ as a function of $\Omega_{\rm s}$ for the canonical parameters for J0045-7319, as evaluated by direct summation of Eq. (16), for four different values of $r_{\rm c}$ (legend, in units of $R_\odot$). The measured $\dot{P} = -3.03 \times 10^{-7}$ is shown by the horizontal dashed line. The vertical black line denotes a rotation rate of 160 km/s, corresponding to the observed projected surface rotation rate $v \sin i = 110$ km/s with an estimated $\sin i \simeq 2^{-1/2}$. The vertical shaded region is the region where $\Omega_{\rm s}$ is less than the breakup rotation rate of the star as a whole, given by $(GM/R^3)^{1/2}$. Each $r_{\rm c}$ is only shown for $|\Omega_{\rm s}| \leq \Omega_{\rm s,c} \equiv (GM_{\rm c}/r_{\rm c}^3)^{1/2}$ the *core* breakup rotation rate.

$R = 6.4R_\odot$ (Kaspi et al. 1996)[3]. The internal structure of the star can be obtained by comparison to detailed stellar structure calculations, yielding $M_{\rm c} \approx 3M_\odot$ and $r_{\rm c} \approx 1.38R_\odot$ (Kumar & Quataert 1998). As the stellar structure may be somewhat uncertain, we take this value $M_{\rm c}$ to be fixed and consider a range of $r_{\rm c} \in [0.7, 1.5]$. In order to compute the orbital decay due to dynamical tides, we also require the ratio $\rho_{\rm c}/\bar{\rho}_{\rm c}$, which can only be obtained via stellar structure simulations. We take $\rho_{\rm c}/\bar{\rho}_{\rm c} \approx 1/3$ as a fiducial value (though in reality this likely changes as $r_{\rm c}$ changes).

Figure 8 shows $\dot{P}$ as a function of $\Omega_{\rm s}$, using Eq. (46), evaluated using four different $r_{\rm c}$. The measured $\dot{P}$ is shown by the horizontal dashed line. Note that for the most compact core radius $r_{\rm c} = 0.7R_\odot$, there are no solutions for $\Omega_{\rm s}$; even a maximally spinning core cannot generate enough tidal dissipation to match the observed $\dot{P}$. In general, substantial retrograde rotation of the stellar core is required to match the observed orbital decay rate, a few times faster than the critical rotation rate of the star as a whole. The required core rotation rate decreases when its radius is increased. The MS star has a projected surface rotation rate of $v \sin i = 113 \pm 10$ km/s (Bell et al. 1995), which is substantially slower than the breakup surface rotation rate of $\sqrt{GM/R} = 512$ km/s. Thus, strong differential rotation is required in the MS star in J0045-7319 to generate the required orbital decay via dynamical tides alone.

5 SUMMARY AND DISCUSSION

In this paper, we have calculated the torque and orbital decay rate due to dynamical tides in a massive, main-sequence (MS) star under the gravitational influence of an eccentric companion. For general eccentricities, these are given by the sums Eqs. (15) and (16) respectively. However, when the eccentricity is large, these sums require the evaluation of many terms to be accurate. We present approximations for two possible regimes:

- For $e \gtrsim 0.3$, we show that the torque and orbital decay rate can be accurately approximated by the integral expressions Eqs. (32) and (41) respectively.
- If furthermore the spin of the stellar core is not near its pseudosynchronized value (i.e. where the torque vanishes; see Section 3.2.2), we show that these two integral expressions can be approximated by the closed-form expressions Eqs. (37) and (46) respectively.

The accuracy of these approximations for the torque and orbital decay rate as functions of the spin of the stellar core and orbit eccentricity are illustrated in Figs. 3, 4, 6, and 7.

We then apply our results to the radio pulsar J0045-7319, which has a MS B star companion and a measured orbital decay rate. In Fig. 8, we show that the required stellar core spin to generate the observed orbital decay is a few times the breakup rotation rate of the entire star. This suggests that the core-envelope coupling timescale in the MS star is at least the characteristic age of the pulsar, ≈ 3 Myr (Kaspi et al. 1996).

Our result can be compared to the result of Kumar & Quataert (1998), where they find that radiative damping of the dynamical tide is insufficient to generate the observed orbital decay, but differential rotation is able to completely dissipate the excited internal gravity waves (IGWs) and generate a sufficiently large tidal torque. By comparison, even though we assume complete dissipation of all IGWs, we further require a core spinning faster than the critical rotation rate of the entire star to generate sufficiently large IGW. One reason for this discrepancy is the suppression of the tidal torque by the terms dependent on $\rho_{\rm c}/\bar{\rho}_{\rm c}$ in Eq. (1). This suppression is omitted in the tidal model of Goldreich & Nicholson (1989) that is used in Kumar & Quataert (1998) Kushnir et al. (as pointed out by 2017), and

[3] Later studies obtain different MS properties in J0045-7319, e.g. Thorsett & Chakrabarty (1999) obtain a MS mass of $M = 10.0M_\odot$ and $M_2 = 1.58M_\odot$. For better comparison with existing work on the effect of dynamical tides in this system, we use the same parameters as earlier works used.

decreases the torque by about a factor of 10–100 depending on the stellar model.

We address a few potential caveats of our tidal model. In our derivations, we have assumed that the stellar spin and orbit axes are aligned. If the stellar obliquity is substantial, then the orbital decay rate is generally expected to be decreased (see e.g. Lai 2012) (NB Dong: is this a good reference? Or do I not need one.). As such, our results give the *maximum* tidal torque and orbital decay rates due to dynamical tides. Additionally, in our work, we have assumed that all Fourier harmonics N excite IGWs at the radiative-convective boundary that damp completely as they propagate towards the stellar surface. This is known to be the case when the normalized tidal forcing frequency satisfies $|2\Omega - 2\Omega_s| \ll \sqrt{GM/R^3}$ (Zahn 1975; Kushnir et al. 2017). In the present scenario, this inequality is always violated for sufficiently large N. However, these higher frequency waves are still likely to deposit most of their angular momentum near the stellar surface, as either their amplitudes grow large and they undergo wave breaking or they encounter a critical layer (Goldreich & Nicholson 1989; though there may be significant reflected angular momentum flux, see Su et al. 2020). In this scenario, significant differential rotation is expected, as the wave breaking process tends to steepen shear flows (Su et al. 2020). This violates the assumption of rigid rotation (see discussion before Eq. 14) but only changes the spin evolution of the star and not the orbital evolution of the binary.

We also discuss potential caveats of our results regarding the pulsar system J0045-7319. We have used the stellar parameters derived by comparison with MS stellar models (Kumar & Quataert 1998). However, it is possible that earlier phases of the binary's evolution have resulted in a B star with stellar structure different than MS stars. If this is the case, the discussion in Section 4 suggests that the core is likely *larger* than MS stellar models predict. Another possible caveat is the accuracy of the original stellar models: a recent study of intermediate and high-mass eclipsing binaries suggests that convective core masses are underpredicted by stellar structure codes (Tkachenko et al. 2020).

5.1 Applicability to Other Tidal Models

[NB Dong: Do you think this is worth pointing out? I think it's worth at least these few sentences, but maybe it scatters the message too much (though I think that the paper isn't very busy as is. . .)]

While the detailed expressions in this work are specific to dynamical tides, the approach of using the Hansen coefficient approximations given by Eq. (19) to evaluate the torque as given by Eq. (9) for a given circular torque $T_{\rm circ}$ is general, i.e.:

$$T = \int_0^\infty C_2^2 N^4 e^{-2N/\eta_2} T_{\rm circ}\left(N\Omega - 2\Omega_s\right)\, {\rm d}N. \tag{47}$$

This can be further simplified analytically for simple $T_{\rm circ}$, e.g. in white dwarfs, $T_{\rm circ}(\omega) \propto \omega^5$ (Fuller & Lai 2012).

6 ACKNOWLEDGEMENTS

We thank Michelle Vick, Christopher O'Connor, and Matteo Cantiello for fruitful discussions. YS is supported by the NASA FINESST grant 19-ASTRO19-0041.

REFERENCES

Alexander M., 1973, Astrophysics and Space Science, 23, 459
Bell J., Bessell M., Stappers B., Bailes M., Kaspi V., 1995, The Astrophysical Journal Letters, 447, L117
Champion D. J., et al., 2008, Science, 320, 1309
Correia A. C., Boué G., Laskar J., Rodríguez A., 2014, Astronomy & Astrophysics, 571, A50
Fuller J., Lai D., 2012, Monthly Notices of the Royal Astronomical Society, 421, 426
Goldreich P., Nicholson P. D., 1989, Astrophysical Journal, 342, 1079
Hurley J. R., Tout C. A., Pols O. R., 2002, Monthly Notices of the Royal Astronomical Society, 329, 897
Hut P., 1981, Astronomy and Astrophysics, 99, 126
Johnston S., Manchester R., Lyne A., Nicastro L., Spyromilio J., 1994, Monthly Notices of the Royal Astronomical Society, 268, 430
Kaspi V., Bailes M., Manchester R., Stappers B., Bell J., 1996, Nature, 381, 584
Kumar P., Quataert E. J., 1998, The Astrophysical Journal, 493, 412
Kushnir D., Zaldarriaga M., Kollmeier J. A., Waldman R., 2017, Monthly Notices of the Royal Astronomical Society, 467, 2146
Lai D., 1996, The Astrophysical Journal Letters, 466, L35
Lai D., 2012, Monthly Notices of the Royal Astronomical Society, 423, 486
Murray C. D., Dermott S. F., 1999, Solar system dynamics. Cambridge university press
Savonije G., Papaloizou J., 1983, Monthly Notices of the Royal Astronomical Society, 203, 581
Stein E. M., Shakarchi R., 2009, Real analysis: measure theory, integration, and Hilbert spaces. Princeton University Press
Storch N. I., Lai D., 2013, Monthly Notices of the Royal Astronomical Society, 438, 1526
Su Y., Lecoanet D., Lai D., 2020, Monthly Notices of the Royal Astronomical Society, 495, 1239
Thorsett S. E., Chakrabarty D., 1999, The Astrophysical Journal, 512, 288
Tkachenko A., et al., 2020, Astronomy & Astrophysics, 637, A60
Vick M., Lai D., Fuller J., 2017, Monthly Notices of the Royal Astronomical Society, 468, 2296
Vigna-Gómez A., MacLeod M., Neijssel C. J., Broekgaarden F. S., Justham S., Howitt G., de Mink S. E., Mandel I., 2020, arXiv preprint arXiv:2001.09829
Zahn J.-P., 1975, Astronomy and Astrophysics, 41, 329
Zahn J.-P., 1977, Astronomy and Astrophysics, 57, 383
Zaldarriaga M., Kushnir D., Kollmeier J. A., 2018, Monthly Notices of the Royal Astronomical Society, 473, 4174

This paper has been typeset from a TEX/LATEX file prepared by the author.